

Origin of non-linear piezoelectricity in III-V semiconductors: Internal strain and bond ionicity from hybrid-functional density functional theory

Miguel A. Caro,^{1,2,3,4,*} Stefan Schulz,¹ and Eoin P. O'Reilly^{1,2}

¹*Photonics Theory Group, Tyndall National Institute, Dyke Parade, Cork, Ireland*

²*Department of Physics, University College Cork, Cork, Ireland*

³*Department of Electrical Engineering and Automation, Aalto University, Espoo, Finland*

⁴*COMP Centre of Excellence in Computational Nanoscience,
Department of Applied Physics, Aalto University, Espoo, Finland*

(Dated: June 14, 2021)

We derive first- and second-order piezoelectric coefficients for the zinc-blende III-V semiconductors, {Al,Ga,In}-{N,P,As,Sb}. The results are obtained within the Heyd-Scuseria-Ernzerhof hybrid-functional approach in the framework of density functional theory and the Berry-phase theory of electric polarization. To achieve a meaningful interpretation of the results, we build an intuitive phenomenological model based on the description of internal strain and the dynamics of the electronic charge centers. We discuss in detail first- and second-order internal strain effects, together with strain-induced changes in ionicity. This analysis reveals that the relatively large importance in the III-Vs of non-linear piezoelectric effects compared to the linear ones arises because of a delicate balance between the ionic polarization contribution due to internal strain relaxation effects, and the contribution due to the electronic charge redistribution induced by macroscopic and internal strain.

I. INTRODUCTION

Non-linear piezoelectricity and its importance in III-V semiconductors and nanostructures has been a topic of intense debate over the last few years.^{1–5} The existence of non-negligible second-order piezoelectricity in GaAs and InAs was first proposed by Bester *et al.*¹ in the context of linear-response density functional theory (DFT). It was soon revisited semi-empirically by Migliorato *et al.*³ using Harrison's bond orbital model and a strain-dependent Kleinman parameter ζ calculated from DFT. More recently, following Bester's methodology, Beya-Wakata *et al.*⁵ have extended the calculation of first- and second-order coefficients to other zinc-blende (ZB) III-V binaries. Although failing for lower band gap materials due to the intrinsic limitations of the local density approximation (LDA),⁶ the approach by Bester *et al.*¹ provides, for the higher energy gap III-V materials, *ab initio* parameters without need to fit to experiment. Given that measuring piezoelectric (PZ) constants accurately is complicated, in particular when possibly large second-order effects are superimposed to the linear ones, the importance of theoretical calculations cannot be overstated. It was indeed found by Beya-Wakata *et al.*,⁵ and is confirmed in the present work with the use of an improved energy functional, that second-order effects are large for the family of ZB III-V materials, in some cases dominating over first-order piezoelectricity even for small strains (e.g. AlP, AlAs and InP). However, it remains unclear and hidden beneath the numbers what is the physical origin of this large second-order PZ effect, and what is the reason for the apparent lack of trends in the evolution of the coefficients for the different compounds.⁵ We try to address this question here by looking separately at the different factors which contribute to the PZ coefficients, investigating separately the linear and nonlinear

contributions to the Kleinman parameter and to the material electronic response, as well as noting the influence of volume effects on the PZ coefficient values.

The form of the second-order PZ polarization tensor for the ZB lattice, along with all the remaining PZ crystal classes, has been established by Grimmer based on symmetry arguments.⁷ The full expression for the PZ vector of a ZB lattice, including first- and second-order effects, reads:⁵

$$\mathbf{P} \equiv e_{14} \begin{pmatrix} \epsilon_4 \\ \epsilon_5 \\ \epsilon_6 \end{pmatrix} + B_{114} \begin{pmatrix} \epsilon_1 \epsilon_4 \\ \epsilon_2 \epsilon_5 \\ \epsilon_3 \epsilon_6 \end{pmatrix} + B_{124} \begin{pmatrix} (\epsilon_2 + \epsilon_3) \epsilon_4 \\ (\epsilon_1 + \epsilon_3) \epsilon_5 \\ (\epsilon_1 + \epsilon_2) \epsilon_6 \end{pmatrix} + B_{156} \begin{pmatrix} \epsilon_5 \epsilon_6 \\ \epsilon_4 \epsilon_6 \\ \epsilon_4 \epsilon_5 \end{pmatrix}, \quad (1)$$

where e_{14} is the linear PZ coefficient, while B_{114} , B_{124} and B_{156} are the second-order PZ coefficients. The strain components are denoted by ϵ_j . We follow standard Voigt notation for all the symbols.

Previous analysis by Beya-Wakata *et al.*,⁵ found that B_{114} and B_{124} show no obvious trend with compound. We note that the two terms in the first (x -) component of the polarization vector [Eq. (1)] involving these two second-order PZ coefficients are proportional to ϵ_1 and $\epsilon_2 + \epsilon_3$, respectively. However, it is often more useful and intuitive to describe the response of a material in terms of the hydrostatic strain $\text{Tr}(\epsilon) = \epsilon_1 + \epsilon_2 + \epsilon_3$ and the biaxial strain $\epsilon_{b,i} = (3\epsilon_i - \text{Tr}(\epsilon))/2$. Equation (1) can

then be rewritten as⁸

$$\mathbf{P} \equiv e_{14} \begin{pmatrix} \epsilon_4 \\ \epsilon_5 \\ \epsilon_6 \end{pmatrix} + A_1 \text{Tr}(\epsilon) \begin{pmatrix} \epsilon_4 \\ \epsilon_5 \\ \epsilon_6 \end{pmatrix} + A_2 \begin{pmatrix} \epsilon_{b,1}\epsilon_4 \\ \epsilon_{b,2}\epsilon_5 \\ \epsilon_{b,3}\epsilon_6 \end{pmatrix} + B_{156} \begin{pmatrix} \epsilon_5\epsilon_6 \\ \epsilon_4\epsilon_6 \\ \epsilon_4\epsilon_5 \end{pmatrix}. \quad (2)$$

with A_1 and A_2 related to the more usual coefficients as follows:

$$A_1 = \frac{B_{114} + 2B_{124}}{3}, \quad A_2 = \frac{2(B_{114} - B_{124})}{3}. \quad (3)$$

While trends in B_{114} and B_{124} alone are difficult to extract,⁵ we find that A_1 and A_2 tend to decrease and to increase, respectively, with increasing unit cell volume. These opposing trends then account for the difficulty to identify any clear trends in B_{114} and B_{124} . Overall, we show that, once the non-linear dependence on strain of the bond polarity, in terms of charge redistribution and internal strain effects, is taken into account, a complete explanation of the PZ effect, including its non linearity, can be provided from first principles alone. We present a consistent picture of ionicity in ZB materials, drawn from the well-established relation between the dynamics of Wannier function centers and electric polarization.⁹ Although data on PZ coefficients is somewhat lacking for ZB semiconductors, more reliable measurements are available for the wurtzite III-Ns. A very recent study of elastic and PZ properties of WZ GaN by Witczak *et al.*¹⁰ serves as validation of the methodology employed here, which we already followed in Refs. 11 and 12, respectively.

Recent work by Tse *et al.*¹³ relying on the Harrison model computed the effective PZ coefficient of GaAs and InAs using a third-order expansion in strain, which corresponds for a fourth-order expansion for the polarization. However, the authors neglected the quadratic contributions arising from shear strain (related to the B_{156} coefficient) which, as we will show, are of the same order of magnitude as the other second-order contributions.

The paper is organized as follows. We introduce our computational method in Sec. II. The main results are then presented in Sec. III. This is followed by an analysis of the results in Sec. IV, where we provide some general considerations in Sec. IV A, before discussing the first-order and second-order coefficients in Secs. IV B and IV C, respectively. Finally, we summarize our conclusions in Sec. V. Some additional details of the calculation method used are presented in the Appendix.

II. COMPUTATIONAL METHOD

Equations (1) and (2) portray all the symmetries applicable to piezoelectricity which are characteristic of the ZB lattice,^{7,14} and therefore form the basis of the target

quantities being calculated here. The DFT calculations for geometry optimization and self-consistent wave functions were carried out using the Heyd-Scuseria-Ernzerhof (HSE) hybrid functional approach^{15,16} within the projector augmented-wave (PAW) method^{17,18} as implemented in the VASP package.¹⁹ The screening parameter μ was fixed to 0.2 in our calculations and the mixing parameter α to 0.25 (these settings correspond to VASP's HSE06 version of the HSE functional). The plane-wave cutoff energy was set to 600 eV. The semicore d states of Ga and In were treated as valence states. A Γ -centered configuration was used for the k -point mesh, with a variable number of divisions. The convergence of the PZ coefficients was found to be slow with respect to the number of \mathbf{k} points, as described further in the Appendix. Table I shows the calculated energy gaps and lattice parameters for all the compounds considered. The calculations of electric polarization were performed employing the Berry-phase technique within the context of the modern theory of polarization,^{9,20–22} as implemented by Martijn Marsman in VASP. We have successfully used a similar approach previously to study internal strain and electric polarization of wurtzite group-III nitrides.^{11,12}

In order to extract the PZ coefficients from the polarization results, we have fit to second-order polynomials. We have performed calculations of P_x for 5 different strain branches $\epsilon^{(i)}$, which read:

$$\begin{aligned} \epsilon^{(1)} &\equiv (0, 0, 0, \beta, \beta, \beta) \rightarrow e_{14} \& B_{156}, \\ \epsilon^{(2)} &\equiv (\alpha, 0, 0, \beta, 0, 0) \rightarrow e_{14} \& B_{114}, \\ \epsilon^{(3)} &\equiv (0, \alpha, 0, \beta, 0, 0) \rightarrow e_{14} \& B_{124}, \\ \epsilon^{(4)} &\equiv (0, \alpha, \alpha, \beta, 0, 0) \rightarrow e_{14} \& B_{124}, \\ \epsilon^{(5)} &\equiv (\alpha, \alpha, \alpha, \beta, \beta, \beta) \rightarrow e_{14}, B_{156} \& \frac{B_{114} + 2B_{124}}{3}. \end{aligned} \quad (4)$$

Here the relation between unstrained and strained structures is given by the strain transformation matrix, which for an arbitrary lattice vector at equilibrium $\mathbf{R}_\alpha \equiv (R_{\alpha,1}, R_{\alpha,2}, R_{\alpha,3})$ is given by

$$\mathbf{R}'_\alpha = \begin{pmatrix} 1 + \epsilon_1 & \frac{\epsilon_6}{2} & \frac{\epsilon_5}{2} \\ \frac{\epsilon_6}{2} & 1 + \epsilon_2 & \frac{\epsilon_4}{2} \\ \frac{\epsilon_5}{2} & \frac{\epsilon_4}{2} & 1 + \epsilon_3 \end{pmatrix} \begin{pmatrix} R_{\alpha,1} \\ R_{\alpha,2} \\ R_{\alpha,3} \end{pmatrix}. \quad (5)$$

We increment the α and β parameters in Eq. (4) so that the Voigt components of the strain tensor follow the relations above and allow to calculate the corresponding PZ coefficients. For branch $\epsilon^{(1)}$ 9 data points per compound and per k mesh were calculated, up to $|\beta| = 0.04$. For the other branches (which involve two-dimensional fitting) 25 data points were used, with $|\alpha|$ and $|\beta|$ up to 0.02 and 0.04, respectively. We have verified that these strain ranges allow a good quality fitting for both linear and quadratic terms, as shown in the Appendix. Obviously this leads to plenty of redundant information which is however useful in order to check consistency between

TABLE I. Direct band gap at Γ , indirect gap (when this is smaller than the direct one) and lattice parameter, for all the binary ZB III-V semiconductors, calculated from the HSE approach as explained throughout the text. A Γ -centered $10 \times 10 \times 10$ k -point sampling is used for all of these calculations.

	Direct gap at Γ (eV)				Indirect gap (eV)				Lattice parameter (\AA)		
	Al	Ga	In		Al	Ga	In		Al	Ga	In
N	5.61	3.10	0.56	N	4.58	n/a	n/a	N	4.365	4.493	4.991
P	4.21	2.81	1.43	P	2.31	2.33	n/a	P	5.471	5.460	5.904
As	2.86	1.33	0.41	As	2.10	n/a	n/a	As	5.687	5.686	6.116
Sb	2.23	0.75	0.31	Sb	1.76	n/a	n/a	Sb	6.188	6.152	6.563

different calculations. These consistency checks are important given the convergence issues with respect to the number of \mathbf{k} points highlighted in the Appendix. They also allow to monitor the effect of symmetry reduction which we have shown to significantly affect the results of calculated elastic and structural properties of semiconductors.²³

III. RESULTS

All our results for first- and second-order PZ coefficients of the 12 ZB binary compounds $\{\text{Al}, \text{Ga}, \text{In}\}-\{\text{N}, \text{P}, \text{As}, \text{Sb}\}$ are summarized in Table II, where we present separately the ionic and electronic contributions to e_{14} , B_{114} , B_{124} , B_{156} , A_1 and A_2 . A number of related results are presented in Fig. 1, and will be discussed in more detail here and in the next section. While trends in B_{114} and B_{124} are difficult to extract,⁵ the magnitude of A_1 shows a clear decrease with increasing unit cell volume and group V row, as shown graphically in Fig. 1. By contrast, A_2 increases for fixed cation with increasing group V row. As mentioned above, Table II presents the ionic and electronic contributions to the different coefficients separately. It is readily clear from the numbers presented, in particular for e_{14} , that the PZ response in ZB arises as the result of two much larger delicately balanced contributions: the ionic and electronic parts. These results are further discussed in Sec. IV B.

Second-order PZ coefficients for the ZB III-V family, except the nitrides, have already been obtained in the DFT frame by Beya-Wakata *et al.* using the LDA.⁵ Our results in Table II are overall very similar for the linear PZ coefficients of the different compounds with wider band gap, but less so for the second-order coefficients, especially for the narrow gap materials. This disagreement is not surprising since the LDA predicts a metallic state for some of these compounds (e.g. GaSb, InAs and InSb) which is not compatible with the existence of a macroscopic electric polarization in the material. Two initial conclusions can be drawn from this comparison and from earlier work on WZ nitrides:¹² i) LDA and/or other DFT approximations can be sufficient to study linear PZ polarization when a positive band gap is correctly predicted and ii) when both schemes predict a positive gap, the

main differences between standard DFT implementations and a hybrid functional approach arise from the disagreement in the predicted internal strain. This second consideration also accounts for the disagreement between LDA-DFT and HSE-DFT in the case of the spontaneous polarization of WZ nitrides, which arises directly from the disagreement regarding the WZ internal parameter u .¹² The HSE approach has been shown to improve upon Kohn-Sham DFT for a wide range of semiconductors regarding the description of not only band gaps, but also lattice parameters and elastic properties.^{11,15,16,24} Therefore we expect also the description of internal strain to be superior when using the HSE functional.

IV. DISCUSSION AND INTERPRETATION OF RESULTS

In the following we discuss the results obtained in this work and interpret them using a simple physical approach. Section IV A briefly comments on separating the system into ionic and electronic parts and the significance of defining a reference starting point. Sections IV B and IV C then consider the results obtained for the first- and second-order piezoelectricity, respectively, and their interpretation within the context of the present model.

A. General considerations

One of the most striking features of piezoelectricity in the ZB III-Vs is that, except for the highly ionic nitrides, the second-order PZ response is very large if compared to the first-order contribution. This assertion becomes extreme in the case of AlP and InP, for which the sign of the effective PZ coefficient as a function of hydrostatic strain $\tilde{e}_{14} = e_{14} + A_1 \text{Tr}(\epsilon)$ would *reverse* its sign for as little as $\approx 0.2\%$ tensile hydrostatic strain. As a matter of fact, Beya-Wakata *et al.*⁵ found a negative linear PZ coefficient for AlP, while our value in Table II is positive. To picture the meaning of this change in sign of the effective PZ coefficient one can imagine a ball-and-stick model in which cations and anions are represented by point charges of opposite sign. A positive \tilde{e}_{14} corresponds to a positively charged cation and a negatively charged anion, which is

TABLE II. All the different first- and second-order PZ coefficients of the ZB III-Vs, split into different contributions. See text for details.

e_{14} (C/m ²)											
	Ionic part: e_{14}^{ion} (C/m ²)				Electronic part: e_{14}^{ele} (C/m ²)				Total: e_{14} (C/m ²)		
	Al	Ga	In		Al	Ga	In		Al	Ga	In
N	-2.266	-2.256	-2.409	N	2.814	2.622	3.002	N	0.548	0.366	0.593
P	-1.553	-1.437	-1.503	P	1.568	1.316	1.518	P	0.014	-0.121	0.016
As	-1.427	-1.313	-1.371	As	1.372	1.108	1.259	As	-0.055	-0.205	-0.111
Sb	-1.236	-1.169	-1.183	Sb	1.141	0.953	1.021	Sb	-0.094	-0.216	-0.161

B_{114} (C/m ²)											
	Ionic part: B_{114}^{ion} (C/m ²)				Electronic part: B_{114}^{ele} (C/m ²)				Total: B_{114} (C/m ²)		
	Al	Ga	In		Al	Ga	In		Al	Ga	In
N	13.08	11.89	11.40	N	-19.89	-17.27	-17.37	N	-6.81	-5.38	-5.96
P	7.06	6.36	6.05	P	-9.08	-7.59	-7.59	P	-2.02	-1.23	-1.54
As	6.38	5.84	5.43	As	-7.99	-6.30	-6.60	As	-1.61	-0.99	-1.17
Sb	5.25	4.88	4.37	Sb	-6.01	-5.18	-5.00	Sb	-0.76	-0.31	-0.62

B_{124} (C/m ²)											
	Ionic part: B_{124}^{ion} (C/m ²)				Electronic part: B_{124}^{ele} (C/m ²)				Total: B_{124} (C/m ²)		
	Al	Ga	In		Al	Ga	In		Al	Ga	In
N	9.78	11.97	9.74	N	-14.83	-18.70	-16.06	N	-5.04	-6.73	-6.32
P	5.98	6.29	5.99	P	-8.75	-9.56	-9.61	P	-2.76	-3.27	-3.62
As	5.41	5.51	5.30	As	-8.00	-8.72	-9.62	As	-2.59	-3.21	-4.31
Sb	4.38	4.29	4.31	Sb	-6.37	-7.06	-8.36	Sb	-1.99	-2.77	-4.04

B_{156} (C/m ²)											
	Ionic part: B_{156}^{ion} (C/m ²)				Electronic part: B_{156}^{ele} (C/m ²)				Total: B_{156} (C/m ²)		
	Al	Ga	In		Al	Ga	In		Al	Ga	In
N	6.32	5.35	3.56	N	-10.46	-8.52	-5.57	N	-4.15	-3.18	-2.00
P	2.98	3.13	2.39	P	-4.42	-4.51	-3.41	P	-1.43	-1.38	-1.02
As	2.82	3.02	2.27	As	-4.14	-4.30	-2.74	As	-1.32	-1.28	-0.46
Sb	2.15	2.41	2.02	Sb	-2.97	-3.11	-2.19	Sb	-0.82	-0.70	-0.16

A_1 (C/m ²)											
	Ionic part: A_1^{ion} (C/m ²)				Electronic part: A_1^{ele} (C/m ²)				Total: A_1 (C/m ²)		
	Al	Ga	In		Al	Ga	In		Al	Ga	In
N	10.88	11.95	10.30	N	-16.52	-18.22	-16.50	N	-5.63	-6.28	-6.20
P	6.34	6.31	6.01	P	-8.86	-8.90	-8.94	P	-2.52	-2.59	-2.93
As	5.73	5.62	5.34	As	-7.99	-7.91	-8.62	As	-2.26	-2.47	-3.27
Sb	4.67	4.48	4.33	Sb	-6.25	-6.44	-7.24	Sb	-1.58	-1.95	-2.90

A_2 (C/m ²)											
	Ionic part: A_2^{ion} (C/m ²)				Electronic part: A_2^{ele} (C/m ²)				Total: A_2 (C/m ²)		
	Al	Ga	In		Al	Ga	In		Al	Ga	In
N	2.20	-0.05	1.10	N	-3.38	0.96	-0.87	N	-1.18	0.90	0.24
P	0.72	0.05	0.04	P	-0.22	1.32	1.34	P	0.49	1.36	1.38
As	0.64	0.22	0.09	As	0.01	1.61	2.02	As	0.65	1.48	2.09
Sb	0.58	0.40	0.04	Sb	0.24	1.25	2.24	Sb	0.82	1.64	2.27

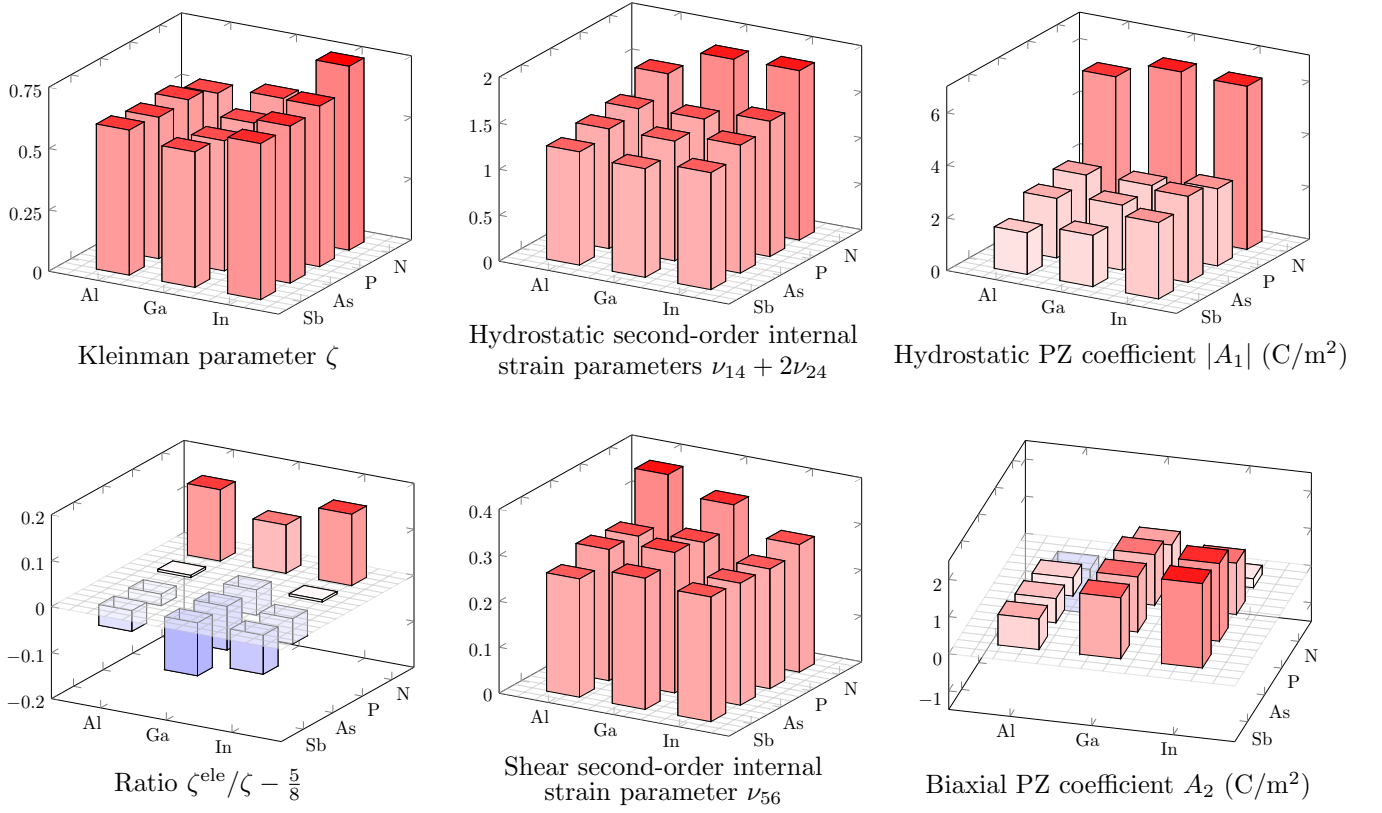


FIG. 1. (Color online) Bar chart with the comparison of different internal strain parameters and PZ coefficients for the different III-V compounds.

found to be the case for the nitrides, implying in the ball-and-stick model a valence electronic charge (to be added to the bare positive core charge) of < 3 electrons on the cation and > 5 electrons on the anion.

This first-order result is then consistent with Harrison's model. In this model the bond polarity depends on the relative magnitude of the covalent interaction U and the difference C in the atomic orbital self-energies on the neighboring atomic sites. The total number of electrons on the cation site increases as the magnitude of the ratio of U/C increases. The large electronegativity of N atoms compared to the other group V elements then leads to a smaller ratio of U/C for the nitrides, consistent with there being > 5 electrons on the N sites in the ball-and-stick model.²⁵ We note however that the calculated negative values of A_1 are contrary to what would be predicted using the Harrison model, where the magnitude of U decreases with increasing bond length, leading to a predicted flow of charge from the cation to the anion with increasing volume. However, the negative value of A_1 describes the opposite behavior – transfer of charge from the anion to the cation with increasing volume.

This disagreement in the direction of charge transfer may reflect factors omitted from the Harrison model, including electron correlation effects. Also, in the context of the modern theory of polarization, a representation in terms of point dipoles lacks rigorous support. Any

attempt to achieve a discrete representation of the system as an ensemble of point charges requires to decouple ionic and electronic contributions, with the point electrons given by the Wannier centers of charge.⁹ For spin-polarized calculations the latter are assigned charge -1 , while in the case of spin degeneracy they are assigned charge -2 . For the III-Vs, the cation has core charge $+3$ and the anion has core charge $+5$. When semicore d states are considered for Ga and In, their core charges become $+13$; however in our discussion we will assume for simplicity that the corresponding extra valence electrons are localized around the core giving an effective core charge of $+3$. Then for ZB III-Vs, in the spin-degenerate case, there are four centers of charge with charge -2 each, corresponding to the overall 8 valence electrons. This is depicted in Fig. 2, for both the case where the cation is chosen to be located at the origin of the unit cell, in which we shall work preferentially since it is the standard representation for ZB, and the case where the anion is located at the origin. Both representations must be (and are) equivalent for computing the polarization. For convenience, the four Wannier centers of charge can be further combined into their center of mass, which is then assigned charge -8 .

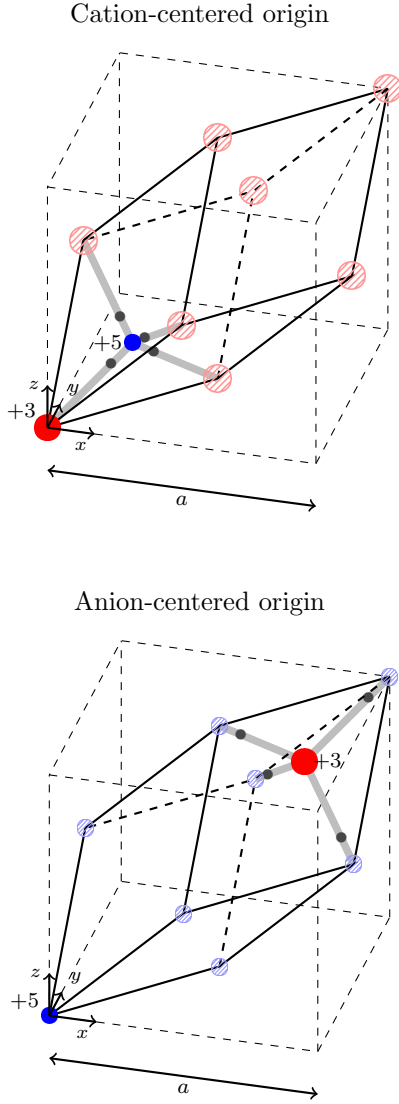


FIG. 2. (Color online) Zinc-blende lattice primitive unit cells showing the underlying cubic symmetry in both cation-at-origin (top) and anion-at-origin (bottom) conventions. Large (red) balls represent cations, with core charge $+3$, while small (blue) balls represent anions, with core charge $+5$. Solid balls are cores contained in the unit cell of the figure and shaded balls are cores contained in neighboring unit cells. The dark dots placed along the bonds represent (spin-degenerate) Wannier centers of charge -2 .

B. First-order internal strain and piezoelectricity

The *ionic* dipole moment in the cation-at-origin representation is given by the relative position of the anion with respect to the cation, which is kept fixed:

$$\mathbf{d}^{\text{ion}} = 5e [(\mathbb{1} + \epsilon)\mathbf{r}_0 + \mathbf{t}]. \quad (6)$$

Here, \mathbf{r}_0 is the position of the anion before strain, and \mathbf{t} is the anion's internal strain, which for ZB is given, *to*

first order, in terms of the Kleinman parameter ζ :^{11,23,26}

$$\mathbf{t}^{(1)} = -\frac{\zeta a}{4} \begin{pmatrix} \epsilon_4 \\ \epsilon_5 \\ \epsilon_6 \end{pmatrix}. \quad (7)$$

The appearance of a strain-dependent part in Eq. (6) is a consequence of the choice of origin to compute the dipole moment, and was already discussed in the seminal paper of Vanderbilt and King-Smith.⁹ Alternatively, if we had placed the origin to compute the dipole moment at a position exactly $5/8$ along the vector connecting the cation and the anion (keeping the same convention for the unit cell), strain dependence would have been removed:

$$\begin{aligned} \mathbf{d}^{\text{ion}} &= 5e \left[(\mathbb{1} + \epsilon) \frac{3\mathbf{r}_0}{8} + \frac{3\mathbf{t}}{8} \right] + 3e \left[(\mathbb{1} + \epsilon) \frac{-5\mathbf{r}_0}{8} \right] \\ &= \frac{15e}{8} \mathbf{t}, \end{aligned} \quad (8)$$

reaching the result that the ionic dipole moment in ZB depends only on internal strain. Therefore any dependence on strain of this value must arise from the dependence of \mathbf{t} on strain. Since the result must be independent of the choice of origin, the ionic dipole moment \mathbf{d}^{ion} can be obtained as in Eq. (6) and then the strain-dependent artifact subtracted. Therefore, in the cation-at-origin convention, using Eqs. (6) and (7) we can express the linear *ionic* PZ coefficient as

$$e_{14}^{\text{ion}} = -\frac{5e}{a^2} \zeta, \quad (9)$$

where the a^2 term appears after dividing by the unit cell's volume $V = a^3/4$.

Conversely, within this same convention, the linear *electronic* PZ coefficient can be expressed as

$$e_{14}^{\text{ele}} = \frac{8e}{a^2} \zeta^{\text{ele}}, \quad (10)$$

which in turn serves as the definition for the “electronic Kleinman parameter” ζ^{ele} . Note that the strain-dependent artifact for the electronic part arises in the same fashion as in Eq. (6) if Wannier centers are used, or arises as the so-called “quantum of polarization” if the computation is done directly from the Berry phase.²²

Finally the total linear PZ coefficient is given by

$$e_{14} = e_{14}^{\text{ion}} + e_{14}^{\text{ele}} = \frac{e}{a^2} (8\zeta^{\text{ele}} - 5\zeta). \quad (11)$$

Within the anion-at-origin convention, the ionic and electronic contributions would have been given by $3e\zeta/a^2$ and $8e(\zeta^{\text{ele}} - \zeta)/a^2$, respectively, thereby, as expected, leaving the total PZ coefficient unaltered.

Equation (11) provides an extremely useful and intuitive insight to the origin of the PZ effect in ZB III-V semiconductors. A net dipole moment in the unit cell appears as a consequence of the loss of centrosymmetry

and can be expressed in terms of the internal strain parameters (see also Ref. 12 for an equivalent treatment in wurtzite). The magnitude of this PZ effect is then given by the ability (or inability) of the Wannier centers of charge to follow the movement of the anion. This idea was already highlighted by Vanderbilt:²⁷ “*the proper piezoelectric response is identically zero for a homogeneous [strain] deformation of both the ionic positions and the Wannier centers*”. Rearranging Eq. (11) as follows allows to emphasize this idea even further:

$$e_{14} = \frac{e\zeta}{a^2} \left(8 \frac{\zeta^{\text{ele}}}{\zeta} - 5 \right), \quad (12)$$

where the ratio ζ^{ele}/ζ characterizes the ability of the Wannier centers of charge to follow the anion core. $\zeta^{\text{ele}}/\zeta = 1$ corresponds to these centers following the core exactly, that is, it depicts an ideal ionic picture where the charge of the anion can be effectively expressed as its oxidation number (-3 in this case). $\zeta^{\text{ele}}/\zeta = 0$ corresponds to the Wannier centers fully ignoring the movement of the anion core and remaining at their original positions in the lattice (plus a strain transformation). This situation would interestingly lead to a larger PZ constant, of negative sign, indicating reversed ionicity, i.e. the centers of charge follow the *cation* movement exactly. For III-Vs, charge balance is achieved when $\zeta^{\text{ele}}/\zeta = 5/8 = 0.625$, in which case the PZ response of the material is zero. The Kleinman parameter for the different compounds is shown in Table III (also in graphical form in Fig. 1), together with the ratio ζ^{ele}/ζ , where ζ^{ele} is obtained from Eq. (10). All the compounds with $\zeta^{\text{ele}}/\zeta > 0.625$ present regular ionicity and a positive PZ coefficient (basically the nitrides), while the rest present reversed ionicity, with a net positive charge on the anions. The proximity of the value of ζ^{ele}/ζ to 0.625 for many of these materials then explains the importance of the quadratic terms in computing the PZ response of the III-Vs, and even in determining its sign.

For comparison, we have computed the numbers for an extreme case of ionicity, ZB NaF, a I-VII compound for which $\zeta = 0.921$ and $\zeta^{\text{ele}}/\zeta = 0.982$, that is the Wannier centers of charge follow the anionic core almost exactly. A Kleinman parameter ζ close to 1 is also indicative of high ionicity because it implies the response of the asymmetric unit to strain is to preserve the tetrahedral bond lengths rather than the bond angles.²⁸

We see from Table III and Fig. 1 that the Kleinman parameter has a relatively small variation across the different III-V compounds considered, although its value does tend to be slightly higher in the In-V compounds, reflecting that the bond-bending force constants are relatively weaker in the In-V compounds compared to the Al- and Ga-containing compounds. We also note that the PZ coefficient of NaF (and other I-VIIIs) is not given by Eq. (12), but by $e_{14} = \frac{e\zeta}{a^2} (8 \frac{\zeta^{\text{ele}}}{\zeta} - 7)$ instead. This analysis allows to establish the maximum linear PZ coefficient that can exist for the different families of binary

TABLE III. Kleinman parameter ζ and ratio of the “electronic Kleinman parameter” ζ^{ele} with respect to ζ for all the III-Vs.

	Kleinman parameter ζ				Ratio ζ^{ele}/ζ		
	Al	Ga	In		Al	Ga	In
N	0.539	0.568	0.749	N	0.776	0.726	0.779
P	0.580	0.535	0.654	P	0.631	0.572	0.631
As	0.576	0.530	0.640	As	0.601	0.527	0.574
Sb	0.591	0.552	0.636	Sb	0.577	0.510	0.539

ZB compounds as a function of their lattice parameter as $e_{14}^{\text{max}} = \frac{Xe}{a^2}$, where X is the absolute value of the anion’s oxidation number. In practice, e_{14} is only close to this value for the I-VII compounds.

Another important consideration that becomes immediately clear from Eq. (12) is the volume effect present in piezoelectricity, whereby the lattice parameter enters the expression of the PZ coefficient as $1/a^2$. This factor varies for the ZB III-V compounds between 0.023 \AA^{-2} for InSb and 0.052 \AA^{-2} for AlN, so that at equal dipole moment per atom pair, this volume effect would enhance the PZ coefficient of AlN by more than a factor of 2 compared to InSb.

C. Second-order internal strain and piezoelectricity

The second-order internal strain parameters in ZB, which we call ν_{ij} , can be obtained in a similar way to the Kleinman parameter²⁶ and the wurtzite internal strain parameters,^{11,29} expanding the expression of the interatomic energy to third-order in strain and evaluating the different terms:

$$\mathbf{t}^{(2)} = a\nu_{14} \begin{pmatrix} \epsilon_1\epsilon_4 \\ \epsilon_2\epsilon_5 \\ \epsilon_3\epsilon_6 \end{pmatrix} + a\nu_{24} \begin{pmatrix} (\epsilon_2 + \epsilon_3)\epsilon_4 \\ (\epsilon_1 + \epsilon_3)\epsilon_5 \\ (\epsilon_1 + \epsilon_2)\epsilon_6 \end{pmatrix} + a\nu_{56} \begin{pmatrix} \epsilon_5\epsilon_6 \\ \epsilon_4\epsilon_6 \\ \epsilon_4\epsilon_5 \end{pmatrix}. \quad (13)$$

Equation (13) can also be expressed in terms of hydrostatic and biaxial strain:

$$\mathbf{t}^{(2)} = a\nu_1 \text{Tr}(\epsilon) \begin{pmatrix} \epsilon_4 \\ \epsilon_5 \\ \epsilon_6 \end{pmatrix} + a\nu_2 \begin{pmatrix} \epsilon_{b,1}\epsilon_4 \\ \epsilon_{b,2}\epsilon_5 \\ \epsilon_{b,3}\epsilon_6 \end{pmatrix} + a\nu_{56} \begin{pmatrix} \epsilon_5\epsilon_6 \\ \epsilon_4\epsilon_6 \\ \epsilon_4\epsilon_5 \end{pmatrix}. \quad (14)$$

It is unsurprising that Eqs. (13) and (14) resemble the expressions of the second-order PZ polarization [cf. Eqs. (1) and (2), respectively]. We will not report their values for

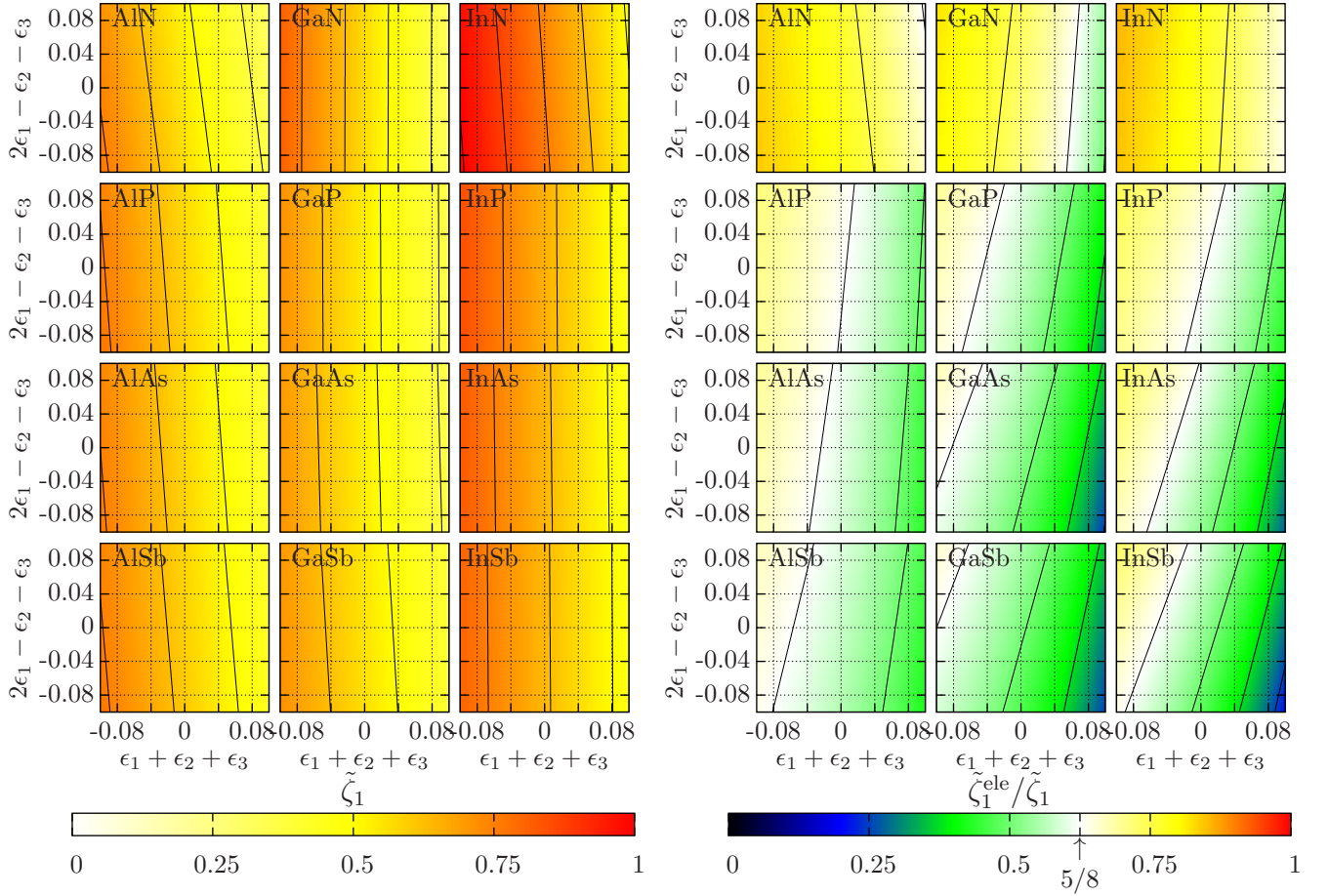


FIG. 3. (Color online) Evolution as a function of hydrostatic and biaxial strain of the strain-dependent Kleinman parameter $\tilde{\zeta}_1$ and $\tilde{\zeta}_1^{\text{ele}}/\tilde{\zeta}_1$ ratio for all the ZB III-V binaries. The distance between adjacent contour lines is 0.125 in the color-coded scale.

all the III-Vs here. They can however be computed from the second-order *ionic* PZ coefficients in Table II in a similar manner to the linear one:

$$\nu_{14} = \frac{a^2}{4} \frac{B_{114}^{\text{ion}} + e_{14}^{\text{ion}}}{5e}, \quad \nu_{24} = \frac{a^2}{4} \frac{B_{124}^{\text{ion}} + e_{14}^{\text{ion}}}{5e},$$

$$\nu_{56} = \frac{a^2}{4} \frac{B_{156}^{\text{ion}}}{5e}, \quad (15)$$

and

$$\nu_1 = \frac{a^2}{4} \frac{A_1^{\text{ion}} + e_{14}^{\text{ion}}}{5e}, \quad \nu_2 = \frac{a^2}{4} \frac{A_2^{\text{ion}}}{5e}, \quad (16)$$

where the term involving e_{14}^{ion} in the different ν s comes from the change in volume due to the hydrostatic strain. Looking at the coefficients for A_1^{ion} , A_2^{ion} and B_{156}^{ion} in Table II, and taking the scaling factor a^2 from Eq. (15) into account, it can be seen that the second-order internal strain shows only a relatively small variation between the different binaries, as was also the case for the Kleinman parameter (Table III and the bar charts in Fig. 1).

The equivalent expressions for the center of mass of

the Wannier centers are:

$$\nu_{14}^{\text{ele}} = \frac{a^2}{4} \frac{B_{114}^{\text{ele}} + e_{14}^{\text{ele}}}{-8e}, \quad \nu_{24}^{\text{ele}} = \frac{a^2}{4} \frac{B_{124}^{\text{ele}} + e_{14}^{\text{ele}}}{-8e},$$

$$\nu_{56}^{\text{ele}} = \frac{a^2}{4} \frac{B_{156}^{\text{ele}}}{-8e}, \quad (17)$$

and

$$\nu_1^{\text{ele}} = \frac{a^2}{4} \frac{A_1^{\text{ele}} + e_{14}^{\text{ele}}}{-8e}, \quad \nu_2^{\text{ele}} = \frac{a^2}{4} \frac{A_2^{\text{ele}}}{-8e}. \quad (18)$$

Using the expression for the second-order internal strain, Eq. (13), together with the first order one, Eq. (7), allows to construct strain-dependent analogues of ζ and ζ^{ele} as a function of hydrostatic and biaxial strain:

$$\tilde{\zeta}_i(\epsilon) = \zeta - 4\nu_1 \text{Tr}(\epsilon) - 4\nu_2 \epsilon_{b,i},$$

$$\tilde{\zeta}_i^{\text{ele}}(\epsilon) = \zeta^{\text{ele}} - 4\nu_1^{\text{ele}} \text{Tr}(\epsilon) - 4\nu_2^{\text{ele}} \epsilon_{b,i}, \quad (19)$$

with

$$\nu_1 = \frac{\nu_{14} + 2\nu_{24}}{3}, \quad \nu_2 = \frac{2\nu_{14} - 2\nu_{24}}{3},$$

$$\nu_1^{\text{ele}} = \frac{\nu_{14}^{\text{ele}} + 2\nu_{24}^{\text{ele}}}{3}, \quad \nu_2^{\text{ele}} = \frac{2\nu_{14}^{\text{ele}} - 2\nu_{24}^{\text{ele}}}{3}. \quad (20)$$

It can be seen from the values of A_1^{ion} and A_2^{ion} in Table II that the magnitude of $\tilde{\zeta}_i(\epsilon)$ tends to increase with decreasing volume ($\text{Tr}(\epsilon) < 0$), as would be expected from the bonds becoming more rigid with decreasing volume. By contrast, $\tilde{\zeta}_i(\epsilon)$ has a much weaker dependence on biaxial strain, $\epsilon_{b,i}$.

We can in addition combine the two terms in Eq. (19) to rewrite Eq. (12) in the following form:

$$\tilde{e}_{14}^i = \frac{e\tilde{\zeta}_i}{a^2} \left(8 \frac{\tilde{\zeta}_i^{\text{ele}}}{\tilde{\zeta}_i} - 5 \right). \quad (21)$$

The second-order contribution to the PZ response then depends both on the evolution of $\tilde{\zeta}_i$ and of $\tilde{\zeta}_i^{\text{ele}}/\tilde{\zeta}_i$: if $\tilde{\zeta}_i^{\text{ele}}/\tilde{\zeta}_i$ was independent of strain then it would be impossible for \tilde{e}_{14}^i to change sign with increasing strain. In Fig. 3 we plot the variation of the strain-dependent parameter $\tilde{\zeta}_i$ (left) and the strain-dependent ratio $\tilde{\zeta}_i^{\text{ele}}/\tilde{\zeta}_i$ (right) for all the ZB III-Vs, as a function of both hydrostatic strain (change in volume) and biaxial strain. We see in the left hand figure for $\tilde{\zeta}_i$ that contours of constant $\tilde{\zeta}_i$ are generally close to vertical, highlighting that the hydrostatic strain has a considerably stronger effect than biaxial strain on the effective Kleinman parameter. The right figure elucidates how strain induces a transition (denoted by the white region in the color maps, for which $\tilde{\zeta}_i^{\text{ele}}/\tilde{\zeta}_i = 5/8$) from a negatively charged to a positively charged anion in all the compounds except for the nitrides (only GaN at very high tensile hydrostatic strain sees this transition for the range shown). For many of the compounds this transition occurs remarkably close to the zero strain region, which highlights the importance of the second-order PZ coefficients. We also note that the contours of constant $\tilde{\zeta}_i^{\text{ele}}/\tilde{\zeta}_i$ are close to vertical for the III-nitrides, becoming more tilted toward the bottom right hand corner of the figure, reflecting the trend previously noted that A_1 tends to decrease and A_2 tends to increase with increasing compound's unit cell volume. It is worth noting also that the nitrides retain their ionic character, a fact that is also reflected in their relatively constant Born effective charge when compared to other III-V compounds.¹²

V. SUMMARY

In summary, we have calculated hybrid-functional first- and second-order PZ coefficients for the whole family of zinc-blende III-V semiconductors. The hybrid-functional approach allows a more accurate evaluation of structural parameters and, more particularly, of band gaps. Other DFT approximations predict a negative band gap for some of these compounds which prevents the calculation of a meaningful electric polarization. We have reported the PZ coefficients split into their ionic and electronic contributions and have shown how the large second-order corrections to the first-order coefficients arise from the

extremely delicate balance between these two large components.

We have built a phenomenological model of the PZ effect in the III-Vs that allows a straightforward interpretation of first- and second-order effects in terms of changes in internal strain and ionicity. While we find changes in internal strain to be largely dominated by hydrostatic strain alone, changes in ionicity are found to be also strongly sensitive to biaxial strain. These changes are more pronounced as the unit cell size increases: they are smallest for AlN and largest for InSb.

ACKNOWLEDGMENTS

The authors acknowledge financial support from Science Foundation Ireland (project numbers 10/IN.1/I2994 and 13/SIRG/2210), the European Union's 7th Framework Programme DEEPEN (Grant Agreement No. 604416), and computational resources from the Tyndall National Institute's in-house computer cluster.

Appendix: Calculation details

The convergence of the electric polarization, and therefore of the PZ coefficients, is rather slow with respect to the number of \mathbf{k} points used in the calculation. This becomes problematic with the highly demanding HSE functional, where typical computational times are one to two orders of magnitude higher than standard implementations of Kohn-Sham DFT. The effect of the finite k sampling on the data affects both the slope at zero strain and the curvature of the polarization, that is first- as well as second-order PZ coefficients. Even for a large number of \mathbf{k} points ($10 \times 10 \times 10$) the derived values are not fully converged. We have found, however, a clear asymptotic behavior as the number of \mathbf{k} points grows, as can be inferred from Fig. 4 for GaSb under homogeneous shear deformation ($\epsilon_4 = \epsilon_5 = \epsilon_6$) for different k grids. The non-zero value of the polarization at zero strain in this case can be observed to be a numerical error due to finite k sampling.³⁰ However, the error is consistent for the different data points within the same series and therefore the extracted PZ coefficients are independent of it. In this context, the values of the extrapolated PZ coefficients have been obtained assigning different weights to the coefficients obtained with different precision, with the lowest weight assigned to those obtained with $4 \times 4 \times 4$ k meshes and the highest weights corresponding to the denser $10 \times 10 \times 10$ k meshes. Intermediate $6 \times 6 \times 6$ and $8 \times 8 \times 8$ meshes have also been considered. In the LDA, an additional number of \mathbf{k} points is specifically required for materials for which a (wrong) negative band gap is predicted, as is the case of GaSb, InN, InAs and InSb. Beya-Wakata *et al.*, for instance, used a very dense $12 \times 12 \times 12$ k mesh to obtain their LDA results.⁵ In our HSE calculations all the III-Vs studied retain a

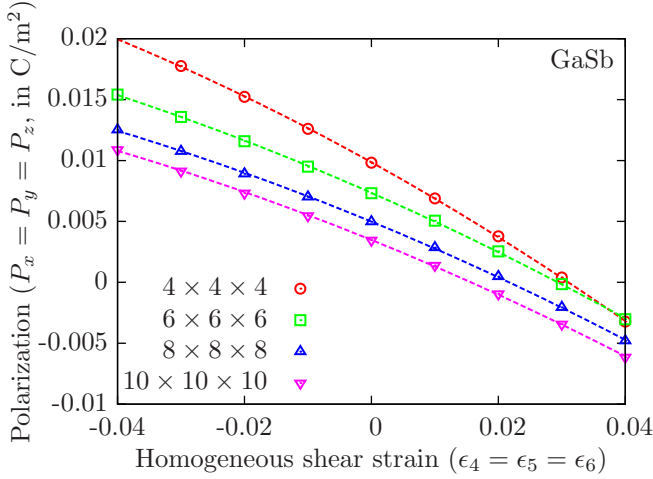


FIG. 4. (Color online) Convergence of the electric polarization values in GaSb as a function of homogeneous shear strain, for different Brillouin zone samplings.

nearly correct (as compared to experiment) positive gap,

as shown in Table I. This renders the matter of k -point density less critical.

To compensate for finite k -mesh sampling, we assume that the absolute value of the numerical error s in either e_{ij} or B_{ijk} due to finite Brillouin zone integration decays exponentially with the number of \mathbf{k} points N_k used in the calculation:

$$|s| = \alpha e^{-\beta N_k}, \quad \alpha, \beta > 0. \quad (\text{A.1})$$

For the linear coefficient e_{14} , we assume the error is 50% for the $4 \times 4 \times 4$ mesh and 1% for the $10 \times 10 \times 10$ mesh. For the non-linear coefficients B_{ijk} these errors are assumed to be 100% and 5%, respectively. These numbers yield $\alpha = 0.653$ and $\beta = 4.18 \times 10^{-3}$ for the linear coefficients and $\alpha = 1.227$ and $\beta = 3.2 \times 10^{-3}$ for the non-linear ones. Then the coefficients are obtained, for each strain branch, as a weighed average of the four available values (corresponding to k -meshes $4 \times 4 \times 4$, $6 \times 6 \times 6$, $8 \times 8 \times 8$ and $10 \times 10 \times 10$), with weights $w(N_k) = 1/s^2$. The final coefficient presented in this paper is obtained as the average of these values between the different strain branches used.

* mcaroba@gmail.com

- ¹ G. Bester, X. Wu, D. Vanderbilt, and A. Zunger, Phys. Rev. Lett. **96**, 187602 (2006).
- ² G. Bester, A. Zunger, X. Wu, and D. Vanderbilt, Phys. Rev. B **74**, 081305 (2006).
- ³ M. A. Migliorato, D. Powell, A. G. Cullis, T. Hammerschmidt, and G. P. Srivastava, Phys. Rev. B **74**, 245332 (2006).
- ⁴ R. Garg, A. H  e, V. Haxha, M. A. Migliorato, T. Hammerschmidt, and G. P. Srivastava, Appl. Phys. Lett. **95**, 041912 (2009).
- ⁵ A. Beya-Wakata, P.-Y. Prodhomme, and G. Bester, Phys. Rev. B **84**, 195207 (2011).
- ⁶ J. P. Perdew and A. Zunger, Phys. Rev. B **23**, 5048 (1981).
- ⁷ H. Grimmer, Acta Crystallogr. Sect. A: Foundations of Crystallography **63**, 441 (2007).
- ⁸ S. Schulz, M. A. Caro, E. P. O'Reilly, and O. Marquardt, Phys. Rev. B **84**, 125312 (2011).
- ⁹ D. Vanderbilt and R. D. King-Smith, Phys. Rev. B **48**, 4442 (1993).
- ¹⁰ P. Witczak, Z. Witczak, R. Jemielniak, M. Kry  sko, S. Krukowski, and M. Bo  kowski, Semicond Sci. Tech. **30**, 035008 (2015).
- ¹¹ M. A. Caro, S. Schulz, and E. P. O'Reilly, Phys. Rev. B **86**, 014117 (2012).
- ¹² M. A. Caro, S. Schulz, and E. P. O'Reilly, Phys. Rev. B **88**, 214103 (2013).
- ¹³ G. Tse, J. Pal, U. Monteverde, R. Garg, V. Haxha, M. A. Migliorato, and S. Tomi  , J. Appl. Phys. **114**, 073515 (2013).
- ¹⁴ J. F. Nye, *Physical properties of crystals: their representation by tensors and matrices* (Oxford University Press,

- Oxford, 1985).
- ¹⁵ J. Heyd, G. E. Scuseria, and M. Ernzerhof, J. Chem. Phys. **118**, 8207 (2003).
- ¹⁶ J. Heyd and G. E. Scuseria, J. Chem. Phys. **121**, 1187 (2004).
- ¹⁷ P. E. Bl  chl, Phys. Rev. B **50**, 17953 (1994).
- ¹⁸ G. Kresse and D. Joubert, Phys. Rev. B **59**, 1758 (1999).
- ¹⁹ G. Kresse and J. Furthm  ller, Phys. Rev. B **54**, 11169 (1996).
- ²⁰ R. D. King-Smith and D. Vanderbilt, Phys. Rev. B **47**, 1651 (1993).
- ²¹ R. Resta, Rev. Mod. Phys. **66**, 899 (1994).
- ²² R. Resta and D. Vanderbilt, "Physics of ferroelectrics: a modern perspective," (Springer-Verlag, Berlin Heidelberg, 2007) Chap. Theory of Polarization: A Modern Approach.
- ²³ M. A. Caro, S. Schulz, and E. P. O'Reilly, J. Phys.: Condens. Matter **25**, 025803 (2013).
- ²⁴ J. Paier, M. Marsman, K. Hummer, G. Kresse, I. C. Gerber, and J. G. Angyan, J. Chem. Phys. **124**, 154709 (2006).
- ²⁵ W. A. Harrison, *Electronic structure and the properties of solids: the physics of the chemical bond* (Dover Publications, 1989).
- ²⁶ P. N. Keating, Phys. Rev. **145**, 637 (1966).
- ²⁷ D. Vanderbilt, J. Phys. Chem. Solids **61**, 147 (2000).
- ²⁸ L. Kleinman, Phys. Rev. **128**, 2614 (1962).
- ²⁹ D. Camacho and Y. M. Niquet, Physica E **42**, 1361 (2010).
- ³⁰ We show the "absolute", in the sense of "branch-independent", value of the polarization. For the centrosymmetric unstrained ZB structure this means the polarization should be ideally zero in the absence of numerical artifacts. See Ref. 27.